Theory of coupled plasmon modes and Fano-like resonances in subwavelength metal structures

Carlo Forestiere,[1,2,*] Luca Dal Negro,[1] and Giovanni Miano[2]

[1]*Department of Electrical and Computer Engineering and Photonics Center, Boston University, 8 Saint Mary's Street, Boston, Massachusetts, USA*

[2]*Department of Electrical Engineering and Information Technology, Università degli Studi di Napoli Federico II, via Claudio 21, Napoli, 80125, Italy*

(Received 12 July 2013; revised manuscript received 13 September 2013; published 10 October 2013)

In this paper, we develop a quasielectrostatic theory describing the coupling of plasmon modes and we discuss its implications for the analysis and the design of the scattering and absorption spectra of complex metal nanostructures. In particular, we show that the interaction of bright plasmon modes determines the onset of zeros in the scattering spectra of nanoscale coupled systems. Under well-defined conditions, these zeros give rise to asymmetric scattering line shapes similar to the spectral signatures described by Ugo Fano in the context of atomic physics. We provide rigorous conditions in which Fano-like resonances occur, and we introduce a method for the direct calculation of their spectral position. In addition, we investigate the role of dark and bright modes in the power absorption near a Fano-like resonance. Our analysis demonstrates the quasielectrostatic origin of Fano-like resonances in subwavelength plasmonic structures.

DOI: 10.1103/PhysRevB.88.155411 PACS number(s): 73.20.Mf, 41.20.Cv, 42.25.Fx

I. INTRODUCTION

In the last few decades, the theory of Ugo Fano[1] concerning a new type of resonant line shape with distinct asymmetry gradually spread beyond the borders of atomic physics, and stimulated a renewed interest in coupled electromagnetic resonances. Wood's anomalies are arguably the most famous electromagnetic phenomena exhibiting the Fano-like asymmetric line shape, but metamaterials, photonic structures, and plasmonic systems also display similar resonances.[2–4] In particular, asymmetric scattering profiles have been recently observed in metal nanostructures excited by an electromagnetic field at optical frequencies, including dolmen-type arrangement,[5,6] ring-disk systems,[7] nanoshells,[8,9] heterodimers,[10] and artificial plasmonic molecules.[11–15] Fano resonances in metal nanostructures have generated large interest, particularly in relation to optical sensors which, taking advantage of the sharp resonant line shape, could potentially offer a significant improvement in sensitivity.

Although extensive experimental and numerical studies of subwavelength complex metal structures have been performed, only few attempts have been done to theoretically describe such resonances.[16–19] Currently, Fano-like resonances are found experimentally or numerically by probing plasmonic nanostructures of complex shapes with radiation of various frequencies and by identifying asymmetric profiles in their scattering spectra. It is therefore highly desirable to develop a rigorous technique for the direct calculation of the frequencies of electromagnetic radiation for which such resonances occur.

In the present work, we derive the theory of coupled plasmon modes in subwavelength plasmonic structures in the quasielectrostatic approximation. The quasielectrostatic approximation is widely used to theoretically investigate plasmonic systems and it has led to important discoveries in this field.[20,21] Our approach is rooted in the boundary eigenvalue problem for the plasmon resonances introduced in Ref. 22 and subsequently extended in Refs. 23–29 and in the concept of bright and dark modes introduced in Ref. 20. In the proposed method, we expand the solution of the nonhomogeneous quasielectrostatic problem in terms of the plasmon modes of the system, and we study the poles and the zeros of the resulting rational function. Thus, we demonstrate how the coupling between at least two bright modes gives rise to Fano-like resonances in the scattering spectrum and to the plasmon equivalent of electromagnetically induced transparency at the Drude damping limit.[5,30–32] Moreover, we provide rigorous conditions in which Fano-like resonances are allowed, a method for the direct calculation of their spectral position and asymmetry degree, and we investigate the dissipation in proximity of a Fano-like resonance. Our analysis demonstrates the quasielectrostatic origin of Fano-like resonances in subwavelength plasmonic structures. This is not surprising given the electrostatic nature of the plasmon resonance.[26,27] Finally, we apply our theory to investigate the Fano-like response of two canonical plasmonic systems.

II. COUPLING OF PLASMON MODES

Let us consider a homogeneous dielectric body of arbitrary shape and relative permittivity $\varepsilon_r(\omega) = \varepsilon_r' - j\varepsilon_r''$, embedded in free-space. We denote with V the volume occupied by the body, with S its boundary, and with L its linear dimension. The outward-pointing normal to the surface S is denoted with $\mathbf{n}$. Assuming that the investigated system is small enough compared to the wavelengths of interest, i.e., $L \ll \lambda$, we employ the quasielectrostatic approximation of the Maxwell's equations.

The source-free electric field that may exist in the presence of a dielectric body with $\varepsilon_r' < 0$ can be described by an equivalent free-standing single layer of electric charge density σ distributed on S. Source-free electric fields exist only when the following homogeneous boundary integral equation has nonzero solutions:[27]

$$\sigma = \beta \mathcal{L}\{\sigma\}, \tag{1}$$

where

$$\mathcal{L}\{\sigma\}(Q) = \frac{1}{2\pi} \oint_S \sigma(M) \frac{\mathbf{r}_{MQ} \cdot \mathbf{n}_Q}{r_{MQ}^3} dS_M. \tag{2}$$

Equation (1) defines an eigenvalue problem in β. Analogously, the source-free electric displacement field that may exist in the presence of a dielectric body with $\varepsilon_r' < 0$ can be described by an equivalent density of double layer of electric charge τ in free space. Source-free electric displacement fields exist only if the equation below has nonzero solutions:[27]

$$\tau = \beta \mathcal{L}^{\dagger}\{\tau\}, \tag{3}$$

where $\mathcal{L}^{\dagger}$ is the adjoint of the operator $\mathcal{L}$,defined as

$$\mathcal{L}^{\dagger}\{\tau\}(Q) = \frac{1}{2\pi} \oint_S \tau(M) \frac{\mathbf{r}_{QM} \cdot \mathbf{n}_M}{r_{QM}^3} dS_M. \tag{4}$$

Since the operators $\mathcal{L}$ and $\mathcal{L}^{\dagger}$ are compact on $\mathbb{L}^2(S)$, they support discrete spectra. Moreover, they share the same eigenvalues $\{\beta_k | k \in \mathbb{N}\}$, whereas their eigenmodes $\{\sigma_k | k \in \mathbb{N}\}$ and $\{\tau_k | k \in \mathbb{N}\}$ form biorthogonal sets:[27]

$$\langle \sigma_k, \tau_j \rangle = \oint_S \sigma_k(M)\, \tau_j(M)\, dS_M = \delta_{kj}. \tag{5}$$

It can be also proved that the eigenvalues are real $\beta_k \in \mathbb{R}$, 1 is an eigenvalue, while the remaining eigenvalues have $|\beta_k| > 1$.[33] However, the eigenvalue $\beta_k = 1$ corresponds to $\varepsilon_r \to \infty$ and it is not relevant to our study.[27] Each eigenmode σ_k generates an electric field $\mathbf{E}_k$ given by

$$\mathbf{E}_k(Q) = \frac{1}{4\pi\varepsilon_0} \oint_S \sigma_k(M) \frac{\mathbf{r}_{MQ}}{r_{MQ}^3} dS_M + \begin{cases} \mathbf{0} & \text{if } Q \notin S, \\ -\frac{\sigma_k}{2\varepsilon_0}\mathbf{n} & \text{if } Q \in S_i, \\ +\frac{\sigma_k}{2\varepsilon_0}\mathbf{n} & \text{if } Q \in S_e, \end{cases} \tag{6}$$

where S_i and S_e denote the internal and external sides of the surface S, respectively. It was demonstrated[27] that the vector fields $\{\mathbf{E}_k | k \in \mathbb{N}\}$ satisfy the strong orthogonality condition $\int_V \mathbf{E}_k \cdot \mathbf{E}_h dV = 0$ if $h \neq k$. In addition, since σ_k is an eigenmode of the problem (1), we obtain from Eq. (6)

$$\mathbf{n} \cdot \mathbf{E}_k = -\frac{1}{2\varepsilon_0} \frac{\beta_k - 1}{\beta_k} \sigma_k \qquad \text{on } S_i. \tag{7}$$

We associate to each eigenmode σ_k a dipole moment $\mathbf{p}_k = (p_{k,x}, p_{k,y}, p_{k,z})$,

$$\mathbf{p}_k = \oint_S \mathbf{r} \sigma_k dS. \tag{8}$$

Since only the modes exhibiting nonzero dipole moment contribute to the far field,[34] we denote the eigenmode σ_k as *bright* if $\mathbf{p}_k \neq \mathbf{0}$, as *dark* otherwise, following the notation introduced in Ref. 20. Using Eq. (7) in Eq. (8) in combination with the divergence theorem, we get

$$\mathbf{p}_k = -2\varepsilon_0 \frac{\beta_k}{(\beta_k - 1)} \int_V \mathbf{E}_k dV. \tag{9}$$

When the dielectric scatterer is excited by an external field $\mathbf{E}^{(i)}$, the *bound* charge density distribution induced on S can be expressed as[27]

$$\sigma(Q) = 2\varepsilon_0 \beta(\omega) \sum_k \frac{\beta_k}{\beta_k - \beta(\omega)} c_k \sigma_k(Q), \tag{10}$$

where[27]

$$\beta(\omega) = \frac{\varepsilon_r(\omega) - 1}{\varepsilon_r(\omega) + 1}, \tag{11}$$

and c_k is the coupling coefficient to the field $\mathbf{E}^{(i)}$,

$$c_k = \langle \mathbf{n} \cdot \mathbf{E}^{(i)}, \tau_k \rangle. \tag{12}$$

It is easy to prove that c_k can be also written as

$$c_k = -\frac{1}{2\varepsilon_0} \frac{(\beta_k - 1)}{\beta_k} \frac{\int_V \mathbf{E}_k \cdot \mathbf{E}^{(i)} dV}{\int_V \|\mathbf{E}_k\|^2 dV}. \tag{13}$$

We say that the eigenmode σ_k is *excitable* by the field $\mathbf{E}^{(i)}$ if $c_k \neq 0$, it is *transparent* to $\mathbf{E}^{(i)}$ if $c_k = 0$. We denote with $\mathbf{p}$ the net dipole moment of the system:

$$\mathbf{p} = \oint_S \mathbf{r} \sigma dS. \tag{14}$$

Combining Eqs. (10) and (14), we have

$$\mathbf{p} = 2\varepsilon_0 \beta(\omega) \sum_k \frac{\beta_k}{\beta_k - \beta(\omega)} c_k \mathbf{p}_k. \tag{15}$$

We denote the quantity $\mathbf{s}_k = c_k \mathbf{p}_k$ as the *radiative strength* of the kth mode under the excitation $\mathbf{E}^{(i)}$ and its component $s_{k,t}$ along the t axis as *t-radiative strength* of the kth mode $\forall t \in \{x, y, z\}$. A similar quantity has already been introduced in Ref. 20. The t-radiative strength can be expressed as

$$s_{k,t} = c_k p_{k,t} = \frac{\int_V \mathbf{E}_k \cdot \mathbf{E}^{(i)} dV}{\int_V \|\mathbf{E}_k\|^2 dV} \int_V \mathbf{E}_k \cdot \hat{\mathbf{t}} dV. \tag{16}$$

In the case of a uniform excitation, e.g., $\mathbf{E}^{(i)} = \hat{\mathbf{x}}$, it is easy to prove that the x-radiative strength of the kth mode of the system $s_{k,x}$ is a non-negative quantity $\forall k \in \mathbb{N}$. Once the total dipole moment is known, the total power scattered by the structure is given by

$$P_{\text{sca}} = \frac{\omega^4}{12\pi\varepsilon_0 c^3} |\mathbf{p}|^2 = \frac{\omega^4}{12\pi\varepsilon_0 c^3} \sum_{t \in \{x,y,z\}} |p_t|^2, \tag{17}$$

being c the speed of light in free space.

The total absorbed power is

$$P_{\text{abs}} = \frac{\varepsilon_0}{2} \omega \varepsilon_r'' \int_V \|\mathbf{E}\|^2 dV, \tag{18}$$

where the total electric field $\mathbf{E}$ within the interior of the volume V is given by

$$\mathbf{E} = \mathbf{E}^{(i)} + 2\varepsilon_0 \beta(\omega) \sum_k \frac{\beta_k}{\beta_k - \beta(\omega)} c_k \mathbf{E}_k, \tag{19}$$

By substituting Eq. (19) in Eq. (18), using the orthogonality of $\mathbf{E}_k$ and Eq. (13), we obtain

$$P_{\text{abs}} = \frac{\varepsilon_0}{2} \omega \varepsilon_r'' \sum_k \left\| \frac{\beta_k (1 - \beta(\omega))}{\beta_k - \beta(\omega)} \right\|^2 d_k, \tag{20}$$

where we have defined the *dissipative strength* of the mode k under the excitation $\mathbf{E}^{(i)}$ as

$$d_k = \frac{\left\| \int_V \mathbf{E}_k \cdot \mathbf{E}^{(i)} dV \right\|^2}{\int_V \|\mathbf{E}_k\|^2 dV}. \tag{21}$$

By comparing Eqs. (13) and (21), we conclude that $d_k = 0$ if and only if the mode k is transparent to the incident field $\mathbf{E}^{(i)}$, thus we have $d_k = 0 \Leftrightarrow c_k = 0 \Rightarrow \mathbf{s_k} = \mathbf{0}$. Therefore all the excitable modes make a contribution to the dissipated power, whereas the modes contributing to the scattered power are only a subset of the excitable modes. In the particular case of uniform excitation, i.e., $\mathbf{E}^{(i)} = \hat{\mathbf{x}}$, we have $d_k = s_{k,x}$, and we can conclude that (i) the dark modes play no role in the power dissipation and (ii) strong (weak) radiative modes correspond to strong (weak) dissipative modes.

The real resonant frequency ω_k corresponding to the mode k can be obtained by equation

$$\mathrm{Re}\{\varepsilon_r(\omega_k)\} = \varepsilon'_{r,k}, \tag{22}$$

where we have defined the resonant permittivity $\varepsilon'_{r,k} \in \mathbb{R}$ associated to the eigenvalue β_k as

$$\varepsilon'_{r,k} = -\frac{\beta_k + 1}{\beta_k - 1}. \tag{23}$$

Using Eq. (23) in Eqs. (15) and (20), we obtain, respectively,

$$\mathbf{p} = \varepsilon_0(1 - \varepsilon_r(\omega)) \sum_k \frac{\varepsilon'_{r,k} - 1}{\varepsilon_r(\omega) - \varepsilon'_{r,k}} \mathbf{s}_k, \tag{24}$$

$$P_{\mathrm{abs}} = \frac{\varepsilon_0}{2} \omega \varepsilon''_r(\omega) \sum_k \left\| \frac{\varepsilon'_{r,k} - 1}{\varepsilon'_{r,k} - \varepsilon_r(\omega)} \right\|^2 d_k. \tag{25}$$

Equations (17), (24), and (25) describe the scattering and the absorption of a plasmonic nanostructure. We notice that in Eq. (24) any component of each term in the summation can assume both positive and negative values, and interference phenomena among different modes are allowed. On the contrary, P_{abs} is the sum of non-negative quantities and interference phenomena are absent. This fact has important consequences on the line shapes of the scattering and absorption spectra, as we will see in the next sections.

We now assume that the dielectric function of the material is described by the Drude model:[35]

$$\varepsilon_r = 1 - \frac{\omega_p^2}{\omega(\omega - j\gamma)}, \tag{26}$$

where ω_p is the plasma frequency and γ is the relaxation frequency. By using Eq. (26) in Eqs. (24) and (25), after some algebra, we obtain

$$\mathbf{p} = -\varepsilon_0 \omega_p^2 \sum_k \frac{\mathbf{s}_k}{\omega^2 - j\gamma\omega - \omega_k^2 - \gamma^2}, \tag{27}$$

$$P_{\mathrm{abs}} = \frac{\varepsilon_0 \omega_p^2 \gamma}{2} \omega^2 \sum_k \frac{d_k}{\left(\omega^2 - \omega_k^2 - \gamma^2\right)^2 + \gamma^2\omega^2}, \tag{28}$$

where ω_k is the real resonant frequency associated to the eigenvalue β_k, i.e.,

$$\omega_k = \sqrt{\omega_p^2 \frac{\beta_k - 1}{2\beta_k} - \gamma^2}. \tag{29}$$

Equations (17), (27), and (28) describe the scattering and the absorption of a Drude-metal nanostructure. They show that, once the resonant frequencies and the radiative and dissipative strengths of all the plasmon modes of a plasmonic system are known, the scattering and the absorption spectra are completely determined. Moreover, they also highlight, in a very clear fashion, how the contribution of each plasmon mode to the scattering and absorption processes is weighted by its radiative and dissipative strengths, respectively.

It is worth noting that, when the dimension of the structure is comparable to the exciting wavelength, the quasielectrostatic approximation becomes inaccurate.[36–38] In this case, the radiation correction introduced in Ref. 27 and experimentally validated in Ref. 39 can be employed to extend its applicability.

A. Scattering in a plasmonic system with two bright and excitable modes: origin of Fano-like resonances

In this section, we derive the expression of the power scattered by a plasmonic system exhibiting two bright and excitable modes. We provide a method for the direct calculation of the zeros of the scattered power, and we unveil their role in the origin of Fano-like line shapes in the scattering spectrum. Thus let us consider a dielectric body excited by the external field $\mathbf{E}^{(i)}$. We assume that the system exhibits only two bright and excitable eigenmodes, i.e., σ_h and σ_k, namely $\mathbf{s}_h, \mathbf{s}_k \neq \mathbf{0}$. No hypothesis is made about the number of dark modes excited. We also assume that the bright eigenmodes are nondegenerate, being associated to two different eigenvalues β_k and β_h with $\beta_k, \beta_h \neq 1$. The resonant permittivities $\varepsilon'_{r,k}, \varepsilon'_{r,h}$ and the real resonant frequencies ω_k, ω_h are associated to the eigenvalues β_k, β_h through Eqs. (23) and (22), respectively.

For the sake of simplicity, we start by considering a Drude metal, then we generalize the treatment to an arbitrary dispersion relation. By using Eq. (27) in the weak relaxation limit, that is, $\gamma^2 \ll \omega_h^2, \omega_k^2$, we obtain after some algebra the expression of the t-component of the net dipole moment of the dielectric body:

$$p_t = -S_t \varepsilon_0 \omega_p^2 \frac{\left(\omega^2 - j\gamma\omega - \omega_{F,t}^2\right)}{\left(\omega^2 - \omega_h^2 - j\gamma\omega\right)\left(\omega^2 - \omega_k^2 - j\gamma\omega\right)}, \tag{30}$$

where $S_t = (s_{h,t} + s_{k,t})$, and we have introduced the *Fano angular frequency* $\omega_{F,t}$ as

$$\omega_{F,t}^2 = \chi_t^{(k,h)} \omega_h^2 + \left(1 - \chi_t^{(k,h)}\right) \omega_k^2 \tag{31}$$

and $\chi_t^{(k,h)}$ is the *asymmetry factor*:

$$\chi_t^{(k,h)} = \frac{s_{k,t}}{s_{h,t} + s_{k,t}}. \tag{32}$$

Each component of the dipolar moment $\mathbf{p}$ is a rational function exhibiting two zeros at the angular frequencies $\pm\omega_{F,t} + j\gamma/2$ and four poles at the frequencies $\pm\omega_h + j\gamma/2$ and $\pm\omega_k + j\gamma/2$. The Fano wavelength $\omega_{F,t}$ is real when $\chi_t^{(k,h)} \leqslant \omega_k^2/(\omega_k^2 - \omega_h^2)$. In this case, when the driving frequency is equal to $\omega_{F,t}$, the real part of the numerator of Eq. (30) vanishes. Provided that no pole-zero cancellation occurs, at the Fano frequency $\omega_{F,t}$, the total dipolar moment along the t axis is *forced-quenched* due to destructive interference between the two plasmon modes, which represent the two channels for the Fano-like interference.[40] If the excitation is uniform, e.g., $\mathbf{E}^{(i)} = \hat{\mathbf{x}}$, both $s_{x,h}$ and $s_{x,k}$ are positive quantities, $\chi_x^{(k,h)}$ belongs to the interval $[0,1]$, and the existence of a real and positive Fano frequency such that $\omega_h \leqslant \omega_{F,x} \leqslant \omega_k$ is always guaranteed.

The total scattered power is obtained substituting Eq. (30) in Eq. (17):

$$P_{\mathrm{sca}} = \frac{\varepsilon_0 \omega^4 \omega_p^4}{12\pi c^3} \frac{\sum_{t\in\{x,y,z\}} S_t^2 \left\| \omega^2 - j\gamma\omega - \omega_{F,t}^2 \right\|^2}{\left\| \omega^2 - \omega_h^2 - j\gamma\omega \right\|^2 \left\| \omega^2 - \omega_k^2 - j\gamma\omega \right\|^2}. \tag{33}$$

The numerator of P_{sca} is the sum of three non-negative quantities, and it can approach zero for very small values of γ in three different cases: (i) when the component of the dipolar moment $\mathbf{p}$ along one axis, e.g., the x axis, is dominant, that is, $S_x \gg S_y, S_z$, and $\omega_{F,x} \in \mathbb{R}$; (ii) when the Fano angular frequencies coincide, i.e., $\omega_{F,x} = \omega_{F,y} = \omega_{F,z} \in \mathbb{R}$; and (iii) when the dipolar moment along one axis is negligible compared to the other two, e.g., $S_z \ll S_y, S_x$ and at the same time the Fano resonances along the remaining two axes coincide, e.g., $\omega_{F,x} = \omega_{F,y} \in \mathbb{R}$. In the following, we investigate in detail only the case (i), assuming $S_x \gg S_y, S_z$. This hypothesis is typically verified when the exciting field is oriented along x axis, as we will show in Sec. III by an example. The remaining two scenarios require only minor modifications of the following treatment. The total scattered power is

$$P_{\mathrm{sca}} \approx \frac{\varepsilon_0 \omega_p^4 \omega^4 S_x^2}{12\pi c^3} \frac{\left\| \omega^2 - j\gamma\omega - \omega_{F,x}^2 \right\|^2}{\left\| \omega^2 - \omega_h^2 - j\gamma\omega \right\|^2 \left\| \omega^2 - \omega_k^2 - j\gamma\omega \right\|^2}. \tag{34}$$

Therefore, at the angular frequency $\omega_{F,x}$, the scattered power is nonzero only due to the Drude damping, in other words we observe a plasmonic analog of electromagnetically induced transparency at the Drude damping limit.[5,30–32] Moreover, as the frequency $\omega_{F,x}$ moves towards one of the two plasmonic resonances, the scattering response becomes highly asymmetric, resembling the Fano line shape.[1]

With the help of Fig. 1 we now analyze the behavior of p_x and of the scattered power P_{sca} using Eqs. (30) and (34), and assuming $\omega_h = 0.2\omega_p$, $\omega_k = 0.3\omega_p$, $\gamma = 0.01\omega_p$, and $S_x \gg S_y, S_z$. We plot the magnitude [Fig. 1(a)] and the phase [Fig. 1(b)] of p_x as a function of the driving (angular) frequency for several values of $\chi_x^{(k,h)}$. As shown in Fig. 1(a), if $\chi_x^{(k,h)} = 0.5$, the two peaks assume different amplitudes whose ratio is $\|p_x(\omega_h)\|/\|p_x(\omega_k)\| \approx (\omega_k/\omega_h)$, while the Fano wavelength $\omega_{F,x}$ lies midway between ω_h and ω_k. As $\chi_x^{(k,h)}$ decreases, i.e., $\chi_x^{(k,h)} < 0.5$, $\|p_x(\omega_h)\|$ further increases with respect to $\|p_x(\omega_k)\|$, and the Fano frequency moves towards ω_k and the profile of $\|p_x\|$ becomes very asymmetric. This fact has a simple interpretation in the case of a uniform excitation, being $s_{h,x}$ and $s_{k,x}$ non-negative quantities: if $\chi_x^{(k,h)} < 0.5$, the x-radiative strength $s_{h,x}$ of the hth mode overwhelms the x-radiative strength $s_{k,x}$ of the kth mode and we can say that the Fano frequency moves towards the weaker bright mode. However, this interpretation cannot be applied to arbitrary excitations, as the sign of the radiative strength cannot be established *a priori*. When the Fano frequency is in very close proximity of ω_k, i.e., $\chi_x^{(k,h)} \ll \gamma\omega_k/(\omega_k^2 - \omega_h^2)$, we observe a pole-zero cancellation in Eq. (30) and the Fano-like shape is no longer visible (case $\chi_x^{(k,h)} = 0.01$ in Fig. 1).

The phase of p_x is plotted in Fig. 1(b). Well isolated poles (zeros) of p_x determine a $-\pi$ (π) shift of the phase for positive values of the driving frequency. This happens in Fig. 1(b) for

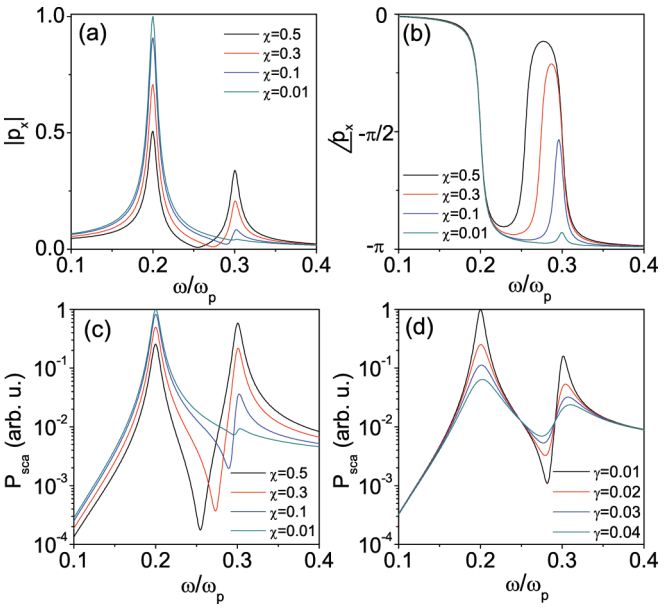

FIG. 1. (Color online) (a) Magnitude and (b) phase of the x component of the dipole moment $\mathbf{p}$ as a function of ω/ω_p in a plasmonic system with two bright and excitable modes, for different values of the asymmetry factor $\chi_x^{(k,h)}$, and assuming $\omega_h = 0.2\omega_p$, $\omega_k = 0.3\omega_p$, and $\gamma = 0.01$. (c) Scattered power spectrum for different values of the asymmetry factor $\chi_x^{(k,h)}$ (semilogarithmic scale). (d) Scattered power spectrum for $\chi_x^{(k,h)} = 0.2$ and for different values of γ.

$\chi_x^{(k,h)} = 0.5$ where the phase undergoes three almost complete shifts of $-\pi$, π, and $-\pi$ due to the action of ω_h, $\omega_{F,x}$, and ω_k, respectively. If $\omega_{F,x}$ is in proximity of ω_k when the driving frequency ω approaches the Fano wavelength $\omega_{F,x}$, $\angle p_x$ starts to increase due to the action of the zero $\omega_{F,x}$ but cannot undergo the full π shift since the action of the pole ω_k brings $\angle p_x$ back to $-\pi$. As a result, the action of $\omega_{F,x}$ and ω_h determines a spike in the phase of p_x [e.g., $\chi_x^{(k,h)} = 0.1$].

We now analyze Eq. (34) with the help of Fig. 1(c) where we plot the scattered power spectrum for our example. When $\chi_x^{(k,h)} = 0.5$, the scattered power exhibits the largest value at the resonance ω_h, being $P_{\mathrm{sca}}(\omega_h)/P_{\mathrm{sca}}(\omega_k) \approx (\omega_h/\omega_k)^3$. Similarly to the analysis carried out for $\|p_x\|$, as we decrease $\chi_x^{(k,h)}$, the Fano wavelength moves towards ω_k and the scattered power spectrum becomes very asymmetric. For very low values of $\chi_x^{(k,h)}$, i.e., $\chi_x^{(k,h)} \ll \gamma\omega_k/(\omega_k^2 - \omega_h^2)$, the pole-zero cancellation prevents us to see the resonance ω_k and the Fano dip.

In order to understand the role of the damping, in Fig. 1(d) we vary the relaxation frequency γ, assuming a fixed value of the asymmetry factor, i.e., $\chi_x^{(k,h)} = 0.2$. Equation (34) indicates that the ratio between the powers $P_{\mathrm{sca}}(\omega_{F,x})$ and $P_{\mathrm{sca}}(\omega_{k,x})$ scales approximately as the fourth power of γ, whereas the ratio between the scattered powers $P_{\mathrm{sca}}(\omega_h)$ and $P_{\mathrm{sca}}(\omega_k)$ does not depend on the relaxation frequency, provided that the two resonant frequencies are well-separated as in the example. Figure 1(d) confirms the very high sensitivity of the Fano profile to the relaxation frequency, showing a smoothing of the Fano profile and an increase of the value of the scattered power at the Fano resonance, as the relaxation frequency γ increases.

The developed treatment can be easily extended to the case of an arbitrary dispersion relation, i.e., $\varepsilon_r = \varepsilon_r(\omega)$. In

this case, the t component of the net dipolar moment of the plasmonic system investigated in this section can be obtained from Eq. (24):

$$p_t = -\varepsilon_0(1-\varepsilon_r(\omega))Z_t \frac{\varepsilon_r(\omega)-\varepsilon'_{F,t}}{(\varepsilon_r(\omega)-\varepsilon'_{r,k})(\varepsilon_r(\omega)-\varepsilon'_{r,h})}, \quad (35)$$

where we have defined the quantity $Z_t = [(1-\varepsilon'_{r,h})s_{h,t} + (1-\varepsilon'_{r,k})s_{k,t}]$ and the Fano permittivity $\varepsilon'_{F,t}$:

$$\varepsilon'_{F,t} = \frac{1}{Z_t}[(1-\varepsilon'_{r,h})s_{h,t}\varepsilon'_{r,k} + (1-\varepsilon'_{r,k})s_{k,t}\varepsilon'_{r,h}]. \quad (36)$$

In correspondence to the real frequency $\omega_{F,t}$ (if exists), at which

$$\mathrm{Re}\{\varepsilon_r(\omega_{F,t})\} = \varepsilon'_{F,t}, \quad (37)$$

the real part of the numerator of Eq. (35) vanishes, and provided that $\mathrm{Im}\{\varepsilon_r(\omega_{F,t})\} \ll \mathrm{Re}\{\varepsilon_r(\omega_{F,t})\}$, the total dipolar moment along the t axis is negligible. In this case, the value of Fano frequency $\omega_{F,t}$ has to be found numerically by solving Eq. (37). It is worth noting that the conditions (36) and (37) are equivalent to Eq. (31) in the case of a Drude metal. The consequences of the cancellation of the numerator of p_x on the scattered spectrum are analogous to the case of the Drude model.

Eventually, we turn our attention to the power dissipated in correspondence to the Fano frequency. Regardless of the dispersion relation, it critically depends on the exciting field. In particular, in the presence of a uniform excitation, e.g., $\mathbf{E}^{(i)} = \hat{\mathbf{x}}$, since $d_k = s_{k,x}$, the two bright modes are exclusively responsible for the system dissipation, thus the absorption spectrum exhibits two peaks in correspondence to the same wavelength ω_h and ω_k. If the excitation is not uniform, the link between the scattering and the dissipation spectra is broken and more complex scenarios can be observed. For instance, a dark mode positioned in proximity of the Fano resonance may determine an high dissipation, in correspondence to very low scattering.

B. Scattering in a plasmonic system with n bright and excitable plasmon modes

It is possible to extend this approach to the general scenario of a plasmonic system exhibiting n bright and excitable eigenmodes $\{\sigma_i | \mathbf{s}_i \neq \mathbf{0} \quad \forall i = 1,\ldots,n\}$ when excited by $\mathbf{E}^{(i)}$. The eigenmodes correspond to n nondegenerate eigenvalues $\{\beta_i | i = 1,\ldots n,\}$. To each eigenvalue we also associate n resonant permittivities $\{\varepsilon'_{r,i} | i = 1,\ldots,n\}$ and n resonant frequencies $\{\omega_i | i = 1,\ldots,n\}$, through Eqs. (23) and (22), respectively.

Assuming, as in the previous section, the x component of the net dipolar moment $\mathbf{p}$ to be dominant within the investigated frequency range, we have $P_{\mathrm{sca}} \approx \frac{\omega^4}{12\pi\varepsilon_0 c^3}\|p_x\|^2$. In this case, P_{sca} approaches zero only when $\|p_x\|$ approaches zero. The x component of $\mathbf{p}$ can be rearranged as a rational function. The values of the angular frequency ω for which the real part of the numerator of p_x vanishes are denoted as Fano frequencies of the system.

For a Drude metal in the weak relaxation limit, it is easy to prove by using Eq. (27) that they are the real roots of the polynomial of degree $2n-2$:

$$\begin{aligned}\mathcal{P}\{\omega_{F,x}\} &= \omega_{F,x}^{(2n-2)}\sum_{i=1}^{n} s_{i,x} - \omega_{F,x}^{(2n-4)}\sum_{i=1}^{n} s_{i,x}e_1\left(\ldots\omega_{i-1}^2,\omega_{i+1}^2\ldots\right)\\ &+ \omega_{F,x}^{(2n-6)}\sum_{i=1}^{n} s_{i,x}e_2\left(\ldots\omega_{i-1}^2,\omega_{i+1}^2\ldots\right)\\ &- \omega_{F,x}^{(2n-8)}\sum_{i=1}^{n} s_{i,x}e_3\left(\ldots\omega_{i-1}^2,\omega_{i+1}^2\ldots\right)+\cdots, \end{aligned} \quad (38)$$

where $e_j(\ldots x_{i-1},x_{i+1}\ldots)$ is an *elementary symmetric polynomial* of degree j in the $n-1$ variables $x_1,\ldots,x_{i-1},x_{i+1},\ldots,x_n$, defined as[41]

$$\begin{aligned} e_0(\ldots x_{i-1},x_{i-1}\ldots) &= 1,\\ e_1(\ldots x_{i-1},x_{i-1}\ldots) &= \sum_{\substack{1\leqslant j\leqslant n\\ j\neq i}} x_j,\\ e_2(\ldots x_{i-1},x_{i-1}\ldots) &= \sum_{\substack{1\leqslant j<k\leqslant n\\ j,k\neq i}} x_j x_k,\\ e_3(\ldots x_{i-1},x_{i-1}\ldots) &= \sum_{\substack{1\leqslant j<k<l\leqslant n\\ j,k,l\neq i}} x_j x_k x_l,\\ &\ldots \end{aligned} \quad (39)$$

In correspondence to the Fano frequencies, provided that no pole-zero cancellation occurs, the total dipolar moment along the x axis approaches zero. In conclusion, Eq. (38) demonstrates that the Fano frequencies of a Drude-metal structure are completely determined by the resonant frequencies and the radiative strengths of the bright and excitable modes of the system. In the case of uniform excitation, i.e., $\mathbf{E}^{(i)} = \hat{\mathbf{x}}$, the x-radiative strength of each mode is non-negative, namely $s_{i,x} \geqslant 0$ and, by using the theorem,[42] we can conclude that the plasmonic system exhibits $n-1$ real Fano frequencies. For an arbitrary excitation, the number of real Fano frequencies needs to be assessed case by case.

The presented treatment can be generalized to an arbitrary dispersion relation, i.e., $\varepsilon_r = \varepsilon_r(\omega)$. In this case, the x component of the net dipolar moment can be rearranged as a rational function in the variable ε_r starting from Eq. (24). In particular, assuming that $\mathrm{Im}\{\varepsilon_r(\omega)\} \ll \mathrm{Re}\{\varepsilon_r(\omega)\}$ within the investigated frequency range, the real part of the numerator of p_x vanishes in correspondence to the real roots of the following polynomial, which are denoted as Fano permittivities:

$$\begin{aligned}\mathcal{Q}\{\varepsilon'_{F,x}\} &= \varepsilon_{F,x}'^{(n-1)}\sum_{i=1}^{n}(1-\varepsilon'_{r,i})s_{i,x}\\ &- \varepsilon_{F,x}'^{(n-2)}\sum_{i=1}^{n}(1-\varepsilon'_{r,i})s_{i,x}e_1(\ldots\varepsilon'_{r,i-1},\varepsilon'_{r,i+1}\ldots)\\ &+ \varepsilon_{F,x}'^{(n-3)}\sum_{i=1}^{n}(1-\varepsilon'_{r,i})s_{i,x}e_2(\ldots\varepsilon'_{r,i-1},\varepsilon'_{r,i+1}\ldots)\\ &- \varepsilon_{F,x}'^{(n-4)}\sum_{i=1}^{n}(1-\varepsilon'_{r,i})s_{i,x}e_3(\ldots\varepsilon'_{r,i-1},\varepsilon'_{r,i+1}\ldots)\\ &+\cdots, \end{aligned} \quad (40)$$

where e_j is defined in Eq. (39). Eventually, the Fano frequencies of the system can be determined through the following equation:

$$\mathrm{Re}\{\varepsilon_r(\omega_{F,x})\} = \varepsilon'_{F,x}. \tag{41}$$

In conclusion, in the case of an arbitrary dispersion relation, the Fano permittivities are completely determined by the resonant permittivities and the radiative strengths of the bright and excitable modes of the system. However, in order to determine the corresponding Fano frequencies of the system an additional equation, i.e., Eq. (41), has to be solved.

C. Absorption in a plasmonic system

In this section, we derive the expression of the absorbed power of a plasmonic system with two excitable modes, demonstrating that each resonance of the absorbed power spectrum can be always described with a Lorentzian line shape. We assume only two nondegenerate modes to be excitable, i.e., $c_h, c_k \neq 0$. They exhibit dissipative strength d_h and d_k, respectively.

In the case of a Drude metal, from Eq. (28), in the weak relaxation limit, we obtain

$$P_{\mathrm{abs}}(\omega) = \gamma \frac{\varepsilon_0 \omega_p^2 \omega^2}{2} \times \frac{(d_k + d_h)\omega^4 - 2\left(d_k\omega_h^2 + d_h\omega_k^2\right)\omega^2 + \left(d_k\omega_h^4 + d_h\omega_k^2\right)}{\left\|\omega^2 - \omega_h^2 - j\gamma\omega\right\|^2 \left\|\omega^2 - \omega_k^2 - j\gamma\omega\right\|^2}. \tag{42}$$

It is easy to prove that for $\omega > 0$, unlike P_{sca}, the rational function P_{abs} does not exhibit any zero with small imaginary part, i.e., proportional to the relaxation frequency of the metal. As a consequence, the oscillations of the numerator of Eq. (42) can only weakly perturb the Lorentzian line shape of the resonances of the absorbed power spectrum, as will be illustrated in Sec. III by two examples. This fact is a consequence of the absence of interference phenomena in the absorbed power. These conclusions can be easily extended to a plasmonic system, with n nondegenerate and excitable modes and to a plasmonic system exhibiting an arbitrary dispersion relation.

III. RESULTS AND DISCUSSION

In this section, we apply our theory to investigate the Fano-like response of two canonical plasmonic systems, namely a quadrumer[12] and a plasmonic dolmen.[5,6] We show that the coupling of bright electrostatic modes in these nanostructures leads to strongly asymmetric resonant line shapes and we determine the positions of the corresponding Fano-like dips. In order to demonstrate the generality of the presented approach we described the dielectric function of the plasmonic quadrumer using the Drude model, while we modeled the dispersion of the dolmen using the experimental data measured for Silver.[43] Moreover, with the help of full-wave electromagnetic codes based on the multiparticle Mie theory[44,45] and on a surface integral formulation[46,47] we investigate the limitations of the quasielectrostatic approach.

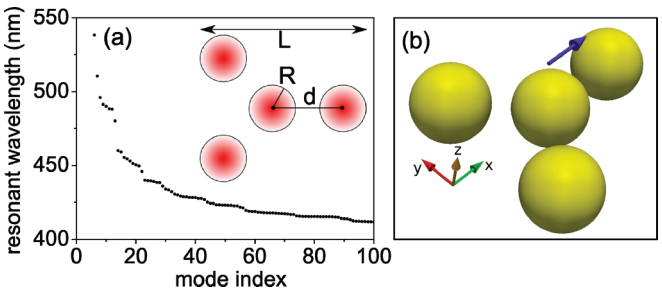

FIG. 2. (Color online) (a) Resonant wavelengths of the modes of the investigated plasmonic oligomer. (b) Sketch of the investigated structure.

We assembled the numerical counterparts of the eigenvalue problems (1) and (3) using the numerical method described in Ref. 27, and improving its precision evaluating the integrals using the techniques described in Ref. 48. The surface of the nanostructure has been discretized with a triangular mesh with N_t triangles. The computation of the eigenvalues and the eigenvectors of two nonsymmetric real matrices of dimensions $N_t \times N_t$, which are the discrete counterparts of the operators $\mathcal{L}$ and $\mathcal{L}^\dagger$, constitutes the bottleneck of the algorithm. This critical calculation has been performed using the LAPACK function DGEEV.[49] The total operation count for both eigenvalues and eigenvectors is asymptotically $\sim 25N_t^3$ (see Ref. 50).

A. Plasmonic oligomer

Let us first consider a plasmonic quadrumer made of four identical nanospheres, placed in correspondence to the vertices and the center of an equilateral triangle, as sketched in Fig. 2. Plasmonic quadrumers have been already investigated experimentally and numerically.[12] They belong to the class of plasmonic *oligomer*, so named because the spatial arrangement of the constituent nanoparticles resembles the arrangement of atoms in a molecule.[11–15] We described the dielectric function of the oligomer using the Drude model with parameters from Ref. 51 ($\omega_p = 6.79 \times 10^{15}$ s^{-1}, $\gamma = 0.25 \times 10^{15}$ s^{-1}). We used a surface mesh with $N_t = 7984$ triangles. We denote with R the radius of each sphere and with d the center-center distance between two adjacent particles (see inset of Fig. 2). Since the integral equations (1) and (3) are invariant with respect to the scaling of the system's dimension, the eigenmodes and the eigenvalues only depend on the ratio d/R. Unless explicitly specified, we consider $d = 2.5R$. By solving the eigenvalue problems of Eqs. (1) and (3), we obtain the eigenvalues set β_i and the eigenmodes σ_i and τ_i. The real resonant wavelengths $\{\lambda_i | i = 1, \ldots, n\}$ (sorted in descending order) are obtained from the eigenvalues using Eq. (29). The first 100 resonant wavelengths are shown in Fig. 2(a).

1. Uniform excitation

In the first part of this section, we consider a uniform excitation, that is, an x-polarized electric field $\mathbf{E}^{(i)}$. The symmetry of the structure and the chosen excitation require the net dipolar moment to be oriented along the x axis. Moreover, since the excitation is uniform, all the excitable modes are bright and thus they make a contribution to the scattered power.

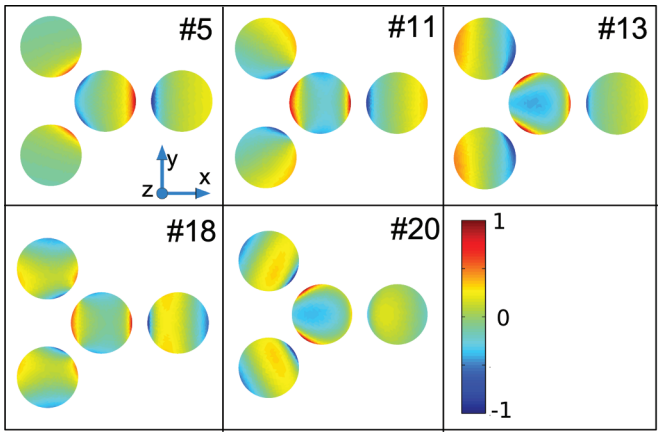

FIG. 3. (Color online) Surface charge density of the bright and excitable eigenmodes (5,11,13,18,20) of the plasmonic oligomer with $d = 2.5R$.

The calculation through Eqs. (8) and (12) of the dipole moments $\mathbf{p}_i$, coupling coefficients c_i, and the corresponding x-radiative strength $s_{i,x}$ reveals that only the modes (5,11,13,18,20), shown in Fig. 3, are bright and excitable by $\mathbf{E}^{(i)}$. Their resonant wavelengths λ_i and x-radiative strengths $s_{i,x}$ (normalized to their maximum) are listed in Table I. All the remaining modes exhibit a negligible value of $|s_x|$, below a fixed threshold δ, set to 0.05. It is worth noting that the dissipative strengths d_i are equal to the corresponding x-radiative strengths. The magnitude of the electric field (defined up to a positive multiplicative factor) of the bright and excitable eigenmodes is plotted in the equatorial plane of the array in Fig. 4.

In order to rigorously predict the position of the Fano wavelengths, we solve Eq. (38) for $n = 5$ using the values of λ_i and $s_{i,x}$ given in Table I, obtaining four Fano wavelengths $\lambda_{F,1}, \ldots, \lambda_{F,4} = \{506, 484, 458, \text{and } 451 \text{ nm}\}$. In Fig. 5(a), we plot the magnitude of p_x calculated using Eq. (27) where the summation index runs over the set {5,11,13,18,20}. We also show the positions of the five resonant wavelengths $\lambda_i | i \in \{5,11,13,18,20\}$ with vertical dashed black lines and the first and the third Fano wavelengths $\lambda_{F,1}$, $\lambda_{F,3}$ with red lines. The remaining Fano wavelengths undergo a pole-zero cancellation with the nearby poles and are not visible. In a first approximation, the Fano wavelength $\lambda_{F,1}$ can be seen as the result of the interaction of the modes {5,11,13}, whereas the Fano-resonance $\lambda_{F,3}$ as the result of the coupling between modes {11,13,18,20}. As expected, we notice that the Fano resonance $\lambda_{F,1}$ is closer to the weaker modes 11,13 than to the stronger mode 5. Similarly, in the coupling between modes

TABLE I. Resonant wavelengths λ_i and x-radiative strengths $s_{i,x}$ (normalized to their maximum) of the bright and excitable modes of the investigated plasmonic oligomer with $d = 2.5R$, illuminated by $\mathbf{E}^{(i)} = \hat{\mathbf{x}}$. The modes with $|s_{k,x}| < \delta = 0.05$ have been disregarded.

Mode index	5	11	13	18	20
λ_i (nm)	546	488	480	453	450
$s_{i,x}$	1	0.26	0.31	0.15	0.06

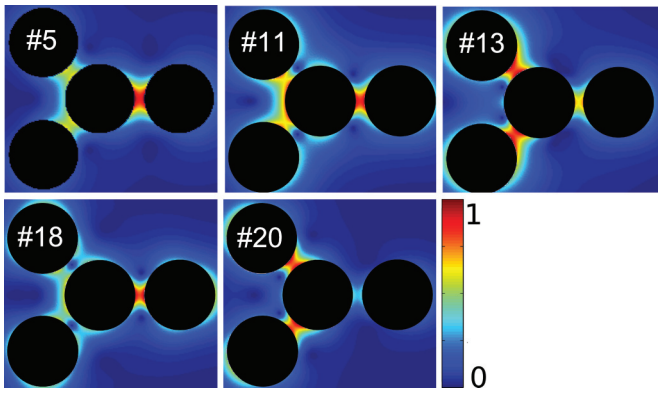

FIG. 4. (Color online) Magnitude of the electric field in the equatorial plane of the array corresponding to the eigenmodes (5,11,13,18,20) of the plasmonic oligomer with $d = 2.5R$.

11,13,18,20, the modes 11,13 are the stronger, while 18,20 are the weaker, as a result, the Fano resonance $\lambda_{F,3}$ is closer to the latter ones.

In Fig. 5(b), we plot the scattered power spectrum P_{sca} calculated using Eq. (17). In order to validate the modal reconstruction approach, we calculate the same quantity using the multiparticle Mie theory (blue-dots).[44,45] We can appreciate a very good agreement between the two approaches. We also notice that the dips of the scattered

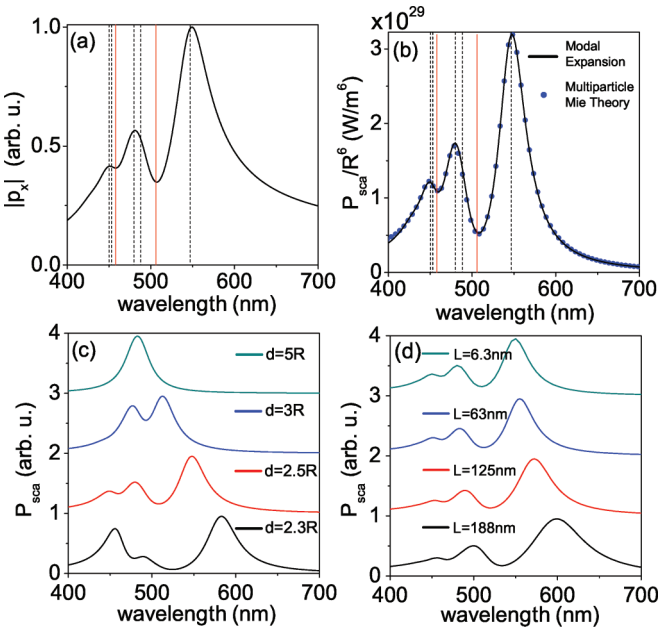

FIG. 5. (Color online) (a) Magnitude $\| p_x \|$ of the x-component of the overall dipolar moment of the plasmonic oligomer with $d = 2.5R$, uniformly excited. The black dashed lines indicates the positions of the resonant wavelengths $\lambda_i | i \in \{5,11,13,18,20\}$. The vertical red lines indicate the position of the Fano wavelengths $\lambda_{F,1}$, $\lambda_{F,3}$. (b) Scattered power P_{sca} by the plasmonic oligomer calculated with the modal approach and with the multiparticle Mie theory for $d = 2.5R$. (c) P_{sca} calculated with the modal approach for several values of the ratio d/R. (d) P_{sca} calculated with the full-wave multiparticles Mie theory for different dimensions L of the structures and for $d = 2.5R$.

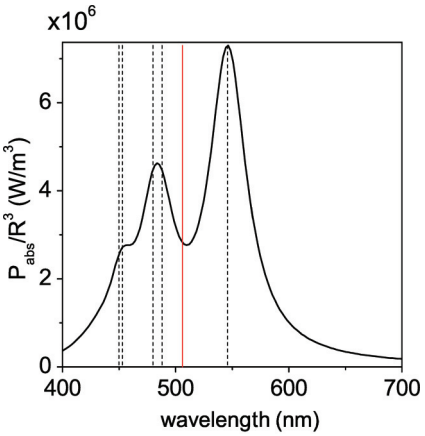

FIG. 6. (Color online) Absorption spectrum P_{abs} of the plasmonic oligomer with $d = 2.5R$, when it is illuminated by $\mathbf{E}^{(i)} = \hat{\mathbf{x}}$.

power correspond to the positions of the Fano wavelengths $\lambda_{F,1}$, $\lambda_{F,3}$, as expected. For the sake of completeness, we also provide the maximum value of the field enhancement, defined as $\texttt{maxFE}(\lambda) = \max_{\mathbf{r}\in\mathbb{R}^3} \frac{\|\mathbf{E}(\mathbf{r},\lambda)\|}{\|\mathbf{E}^{(i)}(\mathbf{r},\lambda)\|}$, in correspondence to the two main peaks of P_{sca}, i.e., $\texttt{maxFE}(546\text{ nm}) = 80$ and $\texttt{maxFE}(484\text{ nm}) = 46$, and in correspondence to the Fano wavelength, i.e., $\texttt{maxFE}(\lambda_{F,1}) = 37$.

In Fig. 5(c), we perform an analysis of the scattered power for different values of d/R. When particles are very far apart ($d/R = 5$), the electromagnetic coupling is negligible, and the response of the system resembles the isolated sphere, where only one (degenerate) eigenvalue is associated to bright eigenmodes. As the ratio d/R decreases, the plasmonic oligomer exhibits two or more nondegenerate eigenvalues with nonzero x-radiative strength and one or more Fano resonances arise.

At this point, it is important to understand the limits of the quasielectrostatic approach. If we introduce the retardation, it is no longer true that the normalized scattering response is independent of the scaling of the system. In Fig. 5(d), we investigate the power scattered by the plasmonic oligomer by scaling its dimension L in the range $L \in [6,188]$ nm (see inset of Fig. 3), by using the full-wave multiparticle Mie theory for $d = 2.5R$. The incident plane wave is propagating along the z axis orthogonally to the array plane. We show that the shape of the curve is qualitatively preserved for dimensions comparable to the wavelength, even if the retardation causes a redshift and a broadening of the resonances.

Eventually, we investigate with the help of Fig. 6 the absorbed power spectrum P_{abs} of the plasmonic oligomer with $d = 2.5R$, when it is illuminated by $\mathbf{E}^{(i)} = \hat{\mathbf{x}}$. The quantity P_{abs} has been calculated by using Eq. (28) where the summation index runs over the set $\{5,11,13,18,20\}$. Since $s_{k,x} = d_k\ \forall k$, the dissipation spectrum exhibits the same resonances of the scattering spectrum, while in correspondence to the Fano wavelength $\lambda_{F,1}$ the absorbed power is in proximity to a local minimum. It is important to notice that, unlike the resonances in the scattered spectrum, the line shapes of the absorbed power are symmetric, since the rational function P_{abs} does not exhibit any zero with imaginary part proportional to the relaxation frequency of the metal.

TABLE II. Resonant wavelengths λ_i and x-radiative strengths $s_{i,x}$ (normalized to their maximum) of the bright and excitable modes of the investigated plasmonic oligomer, illuminated by a dipolar source. The modes with $|s_{k,x}| < \delta = 0.05$ have been disregarded.

Mode index	5	11	13	16	18	31	33
λ_i (nm)	546	488	480	455	453	433	431
$s_{i,x}$	−1	0.1	−0.05	0.11	−0.09	−0.18	−0.12

2. *Dipolar excitation*

We now consider the same plasmonic structure when it is illuminated by a dipolar source. Being the excitation nonuniform, the dissipative strength d_k is no longer equal to the excitation strength $s_{k,x}$. Therefore modes with a large radiative strength can exhibit a small dissipative strength or vice versa, and the excitation of dark modes is allowed. The exciting dipole is positioned atop the central particle at a vertical distance from its center of $2R$ as sketched in Fig. 3(b). Its analytical expression is

$$\mathbf{E}^{(i)}(\mathbf{r}) = \frac{1}{4\pi\varepsilon_0}\left[3\frac{\mathbf{p}\cdot(\mathbf{r}-\mathbf{r}_0)}{\|\mathbf{r}-\mathbf{r}_0\|^5}(\mathbf{r}-\mathbf{r}_0) - \frac{\mathbf{p}}{\|\mathbf{r}-\mathbf{r}_0\|^3}\right], \quad (43)$$

where $\mathbf{p} = (1,0,0)C\,m$ and $\mathbf{r}_0 = (0,0,2R)$. The bright and excitable modes are shown in Table II, together with their x-radiative strength s_x, whereas all the remaining modes exhibit a negligible absolute value of s_x, below a fixed threshold δ, set to 0.05. The number of modes that play a role in the dissipated power is much larger and are reported in Table III with their dissipative strength. Also in this case, the modes with $d_x < \delta$ have been disregarded.

We compute the Fano wavelengths of the scattering spectrum, solving Eq. (38) for $n = 7$, using the values of wavelengths and x-radiative strengths tabulated in Table II, obtaining six Fano wavelengths $\lambda_{F,1},\ldots,\lambda_{F,6} = \{484,484,455,455,449,431\}$ nm. The Fano wavelengths $\lambda_{F,1},\lambda_{F,2}$ undergo a pole-zero cancellation with the nearby plasmon resonance $\lambda_{11},\lambda_{13}$ and neither a peak nor a dip of the scattered power can be found at these wavelengths. In other words, the action of these Fano resonances suppresses the radiated power of the nearby bright resonances. In proximity of 450 nm, we have three zeros $(\lambda_{F,3},\lambda_{F,4},\lambda_{F,5})$ and two poles $\lambda_{16},\lambda_{18}$, thus the overall response resembles the response of an isolated zero, that is a Fano dip. The Fano wavelength $\lambda_{F,6}$ undergoes a cancellation with a nearby pole.

TABLE III. Resonant wavelengths λ_i and dissipative strengths d_i (normalized to their maximum) of the modes contributing to the dissipated power of the investigated plasmonic oligomer, excited by a dipolar source. The modes with $|d_k| < \delta = 0.05$ have been disregarded.

Mode index	5	10	16	19	31	33	34
λ_i (nm)	546	488	455	451	433	431	430
d_i	0.39	0.1	0.66	0.47	0.65	1	0.7
Mode index	41	55	57	58	71	91	
λ_i (nm)	428	422	420	419	417	414	
d_i	0.08	0.57	0.62	0.15	0.06	0.06	

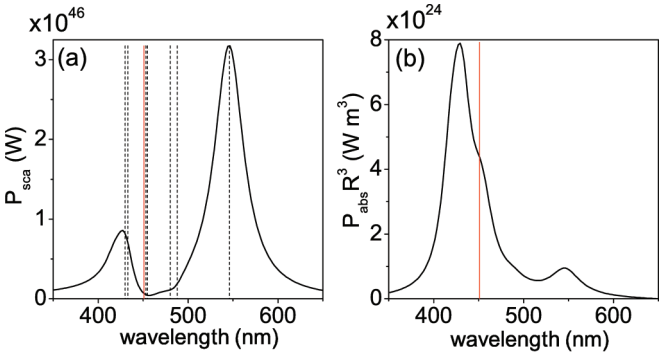

FIG. 7. (Color online) (a) Scattering and (b) absorption spectra of the plasmonic oligomer with $d = 2.5R$, when it is illuminated by a dipolar excitation.

In Fig. 7, we plot the scattered (a) and the absorbed power (b). The only Fano-like dip of the scattered power is shown with a red line. We notice that the absolute maxima of the absorption and scattering occur at different wavelengths. Moreover, in correspondence to the Fano-dip of the scattering spectrum, the action of the modes 16 and 19 results in high dissipation [see Fig. 7(b)]. In particular, the mode 19 exhibits zero dipolar moment along x and does not contribute to the scattered power, while the mode 16 is a radiative mode, whose radiation has been suppressed by the action of a Fano wavelength through a pole-zero cancellation.

In conclusion, using the developed theory, we have investigated the Fano resonances of a plasmonic oligomer for both uniform and nonuniform excitations. In the case of a uniform excitation, due to fact that the dissipative strengths and x-radiative strengths coincide, the scattering and absorption spectra exhibit the same resonances, in addition the Fano resonance is in proximity of a local minimum of the absorption. In the case of a dipolar excitation, the symmetry between the scattering and the dissipation spectra is relaxed and more complex scenarios can be observed. In our example, in correspondence to the Fano resonance, we observe a high dissipation driven by both a bright mode and a mode with zero dipole moment along x.

B. Plasmonic dolmen

We now apply the developed method to study a plasmonic system whose building units are nonspherical particles. We consider a system of three silver nanorods arranged in the configuration sketched in Fig. 8, which is usually referred to as *plasmonic dolmen*.[5,6] We have chosen the geometrical parameters of the dolmen inspired by Ref. 6: $L_1 = 2.3W_1$, $L_2 = 2.6W_1$, $W_2 = 1.15W_1$, $G = 0.35W_1$, $S = 0.5W_1$, and a height along z equal to $h = 0.6W_1$. We used a surface mesh with $N_t = 7996$ triangles. An experimental measured dielectric function for Silver has been used.[43] The dolmen is uniformly excited by an x-polarized electric field $\mathbf{E}^{(i)} = \hat{\mathbf{x}}$.

Solving the eigenvalue problems (1) and (3), we obtain the set of eigenvalues β_i. The resonant permittivities $\{\varepsilon'_{r,i} | i = 1, \ldots, n\}$ are obtained from the eigenvalues using Eq. (23). Then, the resonant wavelengths $\{\lambda_i | i = 1, \ldots, n\}$ (sorted in descending order) are obtained using Eq. (22). The dipolar moment, the coupling coefficient and the radiative-strength of each mode are obtained using Eqs. (8) and (12).

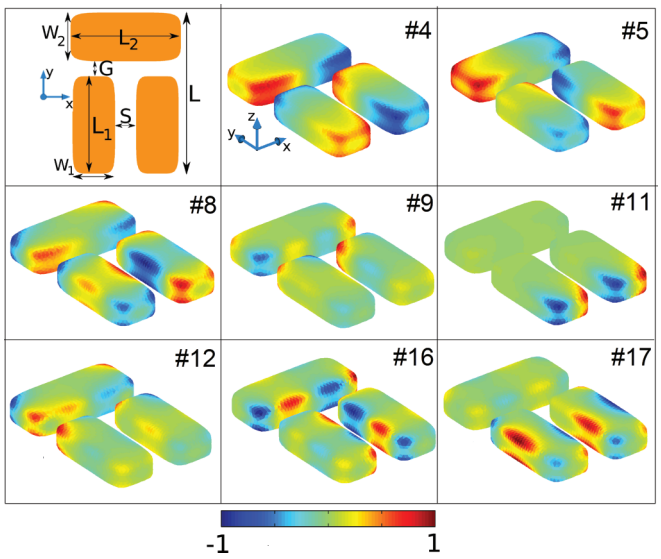

FIG. 8. (Color online) Surface charge density of the bright and excitable eigenmodes (4,5,8,9,11,12,16,17) of the plasmonic dolmen illuminated by $\mathbf{E}^{(i)} = \hat{\mathbf{x}}$.

Within the frequency range considered in this analysis, the components of the net dipole moment along y and z are negligible and the scattered power depends only on p_x. Moreover, only the eight modes {4,5,8,9,11,12,16,17} are bright and excitable by $\mathbf{E}^{(i)} = \hat{\mathbf{x}}$. The corresponding distributions of the charge density and of the magnitude of the electric field are shown in Figs. 8 and 9. Their resonant plasmonic wavelengths λ_i and x-strengths $s_{i,x}$ are listed in Table IV. The remaining modes exhibit a negligible x-radiative strength, being $|s_x|$ below a fixed threshold δ, set to 0.05. In order to evaluate the position of the Fano wavelengths, we have to solve Eqs. (40) and (41) for $n = 8$. However, if we restrict

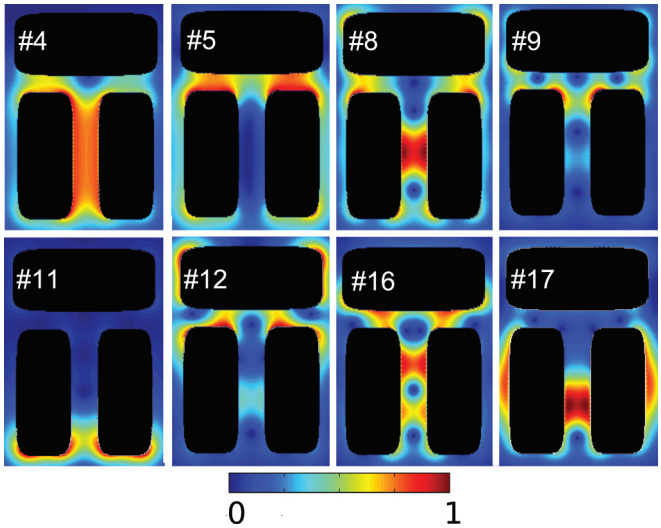

FIG. 9. (Color online) Magnitude of the electric field in the plane of the array corresponding to the eigenmodes (4,5,8,9,11,12,16,17) of the plasmonic dolmen.

TABLE IV. Resonant wavelengths λ_i and x-radiative strengths $s_{i,x}$ (normalized to their maximum) of the bright and excitable modes of the investigated plasmonic dolmen, illuminated by $\mathbf{E}^{(i)} = \hat{\mathbf{x}}$. The modes with $|s_{k,x}| < \delta = 0.05$ have been disregarded.

Mode index	4	5	8	9	11	12	16	17
λ_i (nm)	545	484	390	383	377	373	364	361
$s_{i,x}$	0.42	0.92	0.27	0.24	0.77	0.48	0.26	1

the study to wavelengths $\lambda > 450$ nm, the Fano resonance can be calculated considering only the interaction of the modes 4 and 5, since the remaining modes play only a minor role in this part of the spectrum. Thus, using Eqs. (36) and (37), we obtain the Fano wavelength $\lambda_F \backsimeq 523$ nm.

In Fig. 10(a), we plot the magnitude of p_x obtained using Eq. (24), where the summation is limited to the indices {4,5,8,9,11,12,16,17}. We also show with vertical dashed-black lines the positions of the eight resonant frequencies and with a red line the calculated Fano wavelength. In Fig. 10(b), we plot the scattered power of the system calculated using Eq. (17). The dip of the scattered power corresponds to the position of the Fano wavelength, as expected. Moreover, with the help of Fig. 10(b) we also validate the modal reconstruction method for arrays of nonspherical particles calculating the scattered power using a surface integral formulation

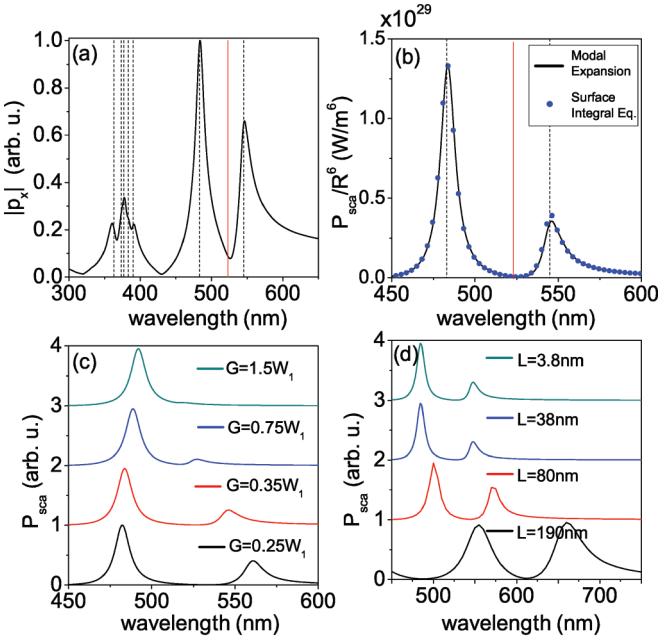

FIG. 10. (Color online) Magnitude $\|p_x\|$ of the x-component of the overall dipole moment of the plasmonic dolmen. The black dashed lines indicates the positions of the resonant wavelengths {4,5,8,9,11,12,16,17}, the red line indicates the position of the Fano resonance λ_F. (b) Corresponding scattered power spectrum calculated with the modal approach and with a surface integral equation method. (c) Scattered power spectrum calculated with the modal approach for several values of the ratio G/W_1. (d) Scattered power spectrum calculated with a full-wave surface integral formulation for different dimensions L of the dolmen.

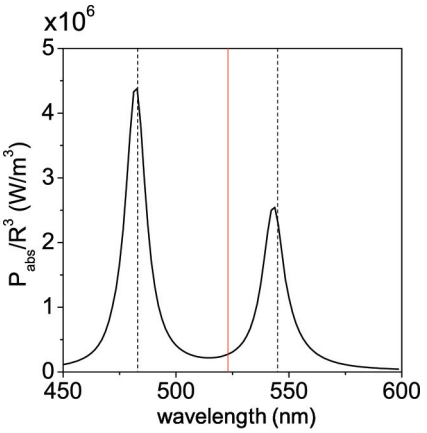

FIG. 11. (Color online) Absorption spectrum P_{abs} of the plasmonic dolmen, when it is illuminated by $\mathbf{E}^{(i)} = \hat{\mathbf{x}}$.

(blue-dots).[46,47] We notice excellent agreement between the two approaches. For completeness, we also provide the values of field enhancement in correspondence to the two peaks of the scattered power spectrum, namely $\texttt{maxFE}(545\text{ nm}) = 103$, $\texttt{maxFE}(484\text{ nm}) = 110$, and in correspondence to the Fano wavelength $\texttt{maxFE}(\lambda_F) = 38$.

In Fig. 10(c), we conduct an analysis of the scattered power for different values of the gap G (see inset in Fig. 8). We observe that when the gap G is very large ($G = 1.5W_1$), the electromagnetic coupling between the rods oriented along the y axis and the rod oriented along the x axis is negligible. Therefore, in this wavelength range, the response of the system resembles the isolated x-oriented nanorod, and only one eigenvalue is associated to a bright and excitable eigenmode. As the value of G decreases, the plasmonic dolmen exhibits for $\lambda > 450$ nm two nondegenerate eigenvalues with nonzero x strength giving rise to a Fano-like resonance.

Eventually, we investigate the limits of the quasielectrostatic approach, introducing the retardation in our analysis. In Fig. 10(d), we plot the scattered power spectrum of the plasmonic dolmen with $G = 0.35W_1$ by scaling its dimension L (defined in the inset of Fig. 8) in the range $L \in [3.8, 190]$ nm and using a full-wave surface integral formulation. The incident plane wave is propagating along the z axis orthogonally to the array plane. We show that the shape of the curve is qualitatively preserved for dimensions comparable to the wavelength, even if the retardation causes a redshift and a broadening of the resonances, confirming the quasielectrostatic origin of Fano-like shapes in plasmonic dolmens.

Eventually, we investigate with the help of Fig. 11 the absorbed power spectrum of the plasmonic dolmen, when it is illuminated by $\mathbf{E}^{(i)} = \hat{\mathbf{x}}$. The quantity P_{abs} has been calculated by using Eq. (25). Since $s_{k,x} = d_k \ \forall k$, the dissipation spectrum exhibits the same resonances of the scattering spectrum, while in correspondence to the Fano wavelength $\lambda_{F,1}$ the absorbed power appears in proximity to a local minimum. In conclusion, unlike the resonances in the scattered spectrum, the line shapes of the absorbed power are symmetric, since no interference process is allowed.

IV. CONCLUSIONS

We derived a quasielectrostatic theory of coupled resonances in subwavelength plasmonic nanostructures. We characterized each plasmon mode by two parameters besides its natural frequency: the radiative strength and the dissipative strength, quantifying the participations of the modes to the scattering and absorption processes, respectively. Then, we expanded the solution of the nonhomogeneous quasielectrostatic problem in terms of the plasmon modes of the system, and we studied the poles and the zeros of the resulting rational function.

We showed that each pole of the scattered power spectrum corresponds to a bright and excitable plasmon mode, while each zero stems from the coupling among all the bright and excitable modes of the system. When a zero exhibits a small imaginary part, i.e., proportional to the relaxation frequency of the metal, provided that no pole-zero cancellation occurs, it gives rise to an asymmetric spectral lineshape in the scattering spectrum and to electromagnetically induced transparency at the Drude damping limit. Instead, when the zero is in close proximity of a plasmon resonance, we observe a pole-zero cancellation, and a suppression of the power radiated by the corresponding mode. Our method allows the direct calculation of the spectral positions of the dips of the scattered power, and of the asymmetry degree of the Fano-like resonance.

In addition, we showed that the absorption spectrum cannot exhibit resonances with a line shape of appreciable asymmetry, because no interference between different modes is allowed in this case. We also showed that in the case of a uniform excitation, dissipative and radiative strengths coincide and strong (weak) dissipative modes correspond to strong (weak) radiative modes, and dark modes play no role. Instead, when the excitation is nonuniform, it is possible to have high absorption at the Fano-dip of the scattering, due to the simultaneous action of dark and bright modes.

Finally, we have applied our theory to investigate the Fano-like response in two canonical plasmonic systems. The approach derived in this paper can be used for the quantitative analysis and design of Fano-like resonances in subwavelength complex plasmonic structures, and can impact the engineering of novel biomedical and chemical nanosensors with enhanced spectral sensitivity.

ACKNOWLEDGMENTS

This work was supported by the U.S. Army Research Laboratory through the Collaborative Research Alliance (CRA) for MultiScale multidisciplinary Modeling of Electronic materials (MSME), by the AFOSR program "Nanoscale Optical Emitters for High Density Information Processing using Photonic-Plasmonic Coupling in Coaxial Nanopillars" under Award FA9550-13-1-0011, and by the Italian Ministry of Education, University and Research through the project PON01_02782.

*Corresponding author: forest@bu.edu

[1] U. Fano, Nuovo Cimento **12**, 154 (1935).
[2] B. Lukyanchuk, N. Zheludev, S. A. Maier, N. J. Halas, P. Nordlander, H. Giessen, and C. T. Chong, Nat. Mater. **9**, 707 (2010).
[3] A. E. Miroshnichenko, S. Flach, and Y. S. Kivshar, Rev. Mod. Phys. **82**, 2257 (2010).
[4] M. Rahmani, B. Luk'yanchuk, and M. Hong, Laser Photonics Rev. **7**, 329 (2013).
[5] S. Zhang, D. A. Genov, Y. Wang, M. Liu, and X. Zhang, Phys. Rev. Lett. **101**, 047401 (2008).
[6] N. Verellen, Y. Sonnefraud, H. Sobhani, F. Hao, V. V. Moshchalkov, P. V. Dorpe, P. Nordlander, and S. A. Maier, Nano Lett. **9**, 1663 (2009).
[7] F. Hao, P. Nordlander, Y. Sonnefraud, P. V. Dorpe, and S. A. Maier, ACS Nano **3**, 643 (2009).
[8] S. Mukherjee, H. Sobhani, J. B. Lassiter, R. Bardhan, P. Nordlander, and N. J. Halas, Nano Lett. **10**, 2694 (2010).
[9] N. T. Fofang, N. K. Grady, Z. Fan, A. O. Govorov, and N. J. Halas, Nano Lett. **11**, 1556 (2011).
[10] L. V. Brown, H. Sobhani, J. B. Lassiter, P. Nordlander, and N. J. Halas, ACS Nano **4**, 819 (2010).
[11] J. A. Fan, C. Wu, K. Bao, J. Bao, R. Bardhan, N. J. Halas, V. N. Manoharan, P. Nordlander, G. Shvets, and F. Capasso, Science **328**, 1135 (2010).
[12] M. Hentschel, M. Saliba, R. Vogelgesang, H. Giessen, A. P. Alivisatos, and N. Liu, Nano Lett. **10**, 2721 (2010).
[13] M. Hentschel, D. Dregely, R. Vogelgesang, H. Giessen, and N. Liu, ACS Nano **5**, 2042 (2011).
[14] D. Dregely, M. Hentschel, and H. Giessen, ACS Nano **5**, 8202 (2011).
[15] F. Shafiei, F. Monticone, K. Q. Le, X.-X. Liu, T. Hartsfield, A. Alu, and X. Li, Nat. Nanotechnol. **8**, 95 (2013).
[16] N. A. Mirin, K. Bao, and P. Nordlander, J. Phys. Chem. A **113**, 4028 (2009).
[17] Z. Ruan and S. Fan, J. Phys. Chem. C **114**, 7324 (2010).
[18] V. Giannini, Y. Francescato, H. Amrania, C. C. Phillips, and S. A. Maier, Nano Lett. **11**, 2835 (2011).
[19] B. Gallinet and O. J. F. Martin, Phys. Rev. B **83**, 235427 (2011).
[20] M. I. Stockman, S. V. Faleev, and D. J. Bergman, Phys. Rev. Lett. **87**, 167401 (2001).
[21] K. Li, M. I. Stockman, and D. J. Bergman, Phys. Rev. Lett. **91**, 227402 (2003).
[22] F. Ouyang and M. Isaacson, Ultramicroscopy **31**, 345 (1989).
[23] F. Ouyang and M. Isaacson, Philos. Mag. B **60**, 481 (1989).
[24] F. J. Garcia de Abajo and J. Aizpurua, Phys. Rev. B **56**, 15873 (1997).
[25] F. J. Garcia de Abajo and A. Howie, Phys. Rev. Lett. **80**, 5180 (1998).
[26] D. R. Fredkin and I. D. Mayergoyz, Phys. Rev. Lett. **91**, 253902 (2003).
[27] I. Mayergoyz, D. Fredkin, and Z. Zhang, Phys. Rev. B **72**, 155412 (2005).
[28] I. D. Mayergoyz, Z. Zhang, and G. Miano, Phys. Rev. Lett. **98**, 147401 (2007).
[29] T. J. Davis, K. C. Vernon, and D. E. Gómez, Phys. Rev. B **79**, 155423 (2009).

[30]C. L. G. Alzar, M. A. G. Martinez, and P. Nussenzveig, Am. J. Phys. **70**, 37 (2002).
[31]N. Liu, L. Langguth, T. Weiss, J. Kastel, M. Fleischhauer, T. Pfau, and H. Giessen, Nat. Mater. **8**, 758 (2009).
[32]S. I. Bozhevolnyi, A. B. Evlyukhin, A. Pors, M. G. Nielsen, M. Willatzen, and O. Albrektsen, New J. Phys. **13**, 023034 (2011).
[33]O. D. Kellogg, *Foundations of Potential Theory* (McGraw-Hill, New York, 1929).
[34]J. Jackson, *Classical Electrodynamics* (Wiley & Sons, New York, 1998).
[35]C. F. Bohren and D. R. Huffman, *Absorption and Scattering of Light by Small Particles* (Wiley & Sons, New York, 1998).
[36]V. Myroshnychenko, J. Rodriguez-Fernandez, I. Pastoriza-Santos, A. M. Funston, C. Novo, P. Mulvaney, L. M. Liz-Marzan, and F. J. Garcia de Abajo, Chem. Soc. Rev. **37**, 1792 (2008).
[37]B. Rolly, B. Stout, and N. Bonod, Phys. Rev. B **84**, 125420 (2011).
[38]C. Gao, J. Vuong, Q. Zhang, Y. Liu, and Y. Yin, Nanoscale **4**, 2875 (2012).
[39]L. Hung, S. Y. Lee, O. McGovern, O. Rabin, and I. Mayergoyz, Phys. Rev. B **88**, 075424 (2013).
[40]Y. S. Joe, A. M. Satanin, and C. S. Kim, Phys. Scripta **74**, 259 (2006).
[41]P. Borwein and T. Erdelyi, *Polynomials and Polynomial Inequalities* (Springer-Verlag, New York, 1995).
[42]D. C. Kurtz, Am. Math. Mon. **99**, 259 (1992).
[43]P. B. Johnson and R. W. Christy, Phys. Rev. B **6**, 4370 (1972).
[44]J. Bruning and Y. Lo, IEEE Antennas Propag. **19**, 378 (1971).
[45]Y. lin Xu, Appl. Opt. **34**, 4573 (1995).
[46]R. Harrington, *Field Computation by Moment Methods* (Macmillan, New York, 1968).
[47]C. Forestiere, G. Iadarola, G. Rubinacci, A. Tamburrino, L. Dal Negro, and G. Miano, J. Opt. Soc. Am. A **29**, 2314 (2012).
[48]R. Graglia, IEEE Antennas Propag. **41**, 1448 (1993).
[49]E. Anderson, Z. Bai, C. Bischof, S. Blackford, J. Demmel, J. Dongarra, J. Du Croz, A. Greenbaum, S. Hammarling, A. McKenney, and D. Sorensen, *LAPACK Users' Guide* (Society for Industrial and Applied Mathematics, Philadelphia, 1999).
[50]W. H. Press, S. A. Teukolsky, W. T. Vetterling, and B. P. Flannery, *Numerical Recipes 3rd Edition: The Art of Scientific Computing* (Cambridge University Press, New York, 2007).
[51]S. A. Maier, P. G. Kik, and H. A. Atwater, Phys. Rev. B **67**, 205402 (2003).